NANO LETTERS

LETTER

pubs.acs.org/NanoLett

Reconfigurable Imaging Systems Using Elliptical Nanowires

Ethan Schonbrun,*,† Kwanyong Seo,‡ and Kenneth B. Crozier‡

†Rowland Institute for Science, Harvard University, 100 Edwin H. Land Boulevard, Cambridge, Massachusetts 02142, United States

‡School of Engineering and Applied Sciences, Harvard University, 29 Oxford Street, Cambridge, Massachusetts 02138, United States

S Supporting Information

ABSTRACT: Materials that have subwavelength structure can add degrees of freedom to optical system design that are not possible with bulk materials. We demonstrate two lenses that are composed out of lithographically patterned arrays of elliptical cross-section silicon nanowires, which can dynamically reconfigure their imaging properties in response to the polarization of the illumination. In each element, two different focusing functions are polarization encoded into a single lens. The first nanowire lens has a different focal length for each linear polarization state, thereby realizing the front end of a nonmechanical zoom imaging system. The second nanowire lens has a different optical axis for each linear polarization state, demonstrating stereoscopic image capture from a single physical aperture.

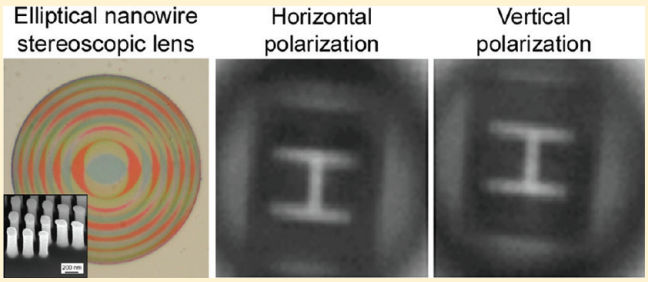

KEYWORDS: Artificial dielectrics, nanowires, diffractive optics, birefringence

The miniaturization and integration of optical components has enabled imaging systems to appear in many new areas. For example, medicine has seen several advances in endoscopy and other small form factor microscopes for in situ inspection. In addition, extremely compact cameras threaten to redefine consumer photography and machine vision. Miniaturized optical imaging systems can often obtain performance competitive with larger bulk systems in terms of resolution and aberration correction.[1] What is frequently lost in miniaturized imaging systems, however, is the flexibility and functionality of larger systems. Traditionally, much of an imaging system's functionality is based on dynamic positioning of the lens with respect to the image sensor. Both focusing and changing the magnification, for example, require mechanical motion or swapping of lenses and are consequently frequently abandoned in miniaturized systems.

One possibility for adding functionality to compact imaging systems is using active elements based on liquid crystals,[2] micromirror arrays,[3] or deformable mirrors.[4] These systems have an extremely large number of degrees of freedom, owing to their large pixel count, and consequently can perform an enormous number of different optical functions. Their drawback, however, is that they require electrical connections to address each of the individual pixels which adds complexity and bulk to the miniaturized optical system. Other promising directions are the implementation of liquid lenses that use the physical boundary between two immiscible fluids for refraction, where the shape of the boundary can be controlled electronically.[5] For applications that require a continuous change of focal length, such as autofocus, liquid lenses are effective. Yet there are many surface profiles that are inaccessible due to the physics of surface tension, for example, high numerical aperture lenses and other aspherical surfaces.

Holography offers another method for adding functionality to an optical system. Instead of changing their optical properties as a function of time, holograms can be designed to have properties that vary as a function of wavelength or incident angle. This feature of volume holograms, called Bragg selectivity, has primarily been taken advantage of in optical data storage schemes[6] and the storage of images for projection.[7] Recently there has also been interest in holographic imaging systems that use Bragg selectivity to encode multiple filters into the same volume element.[8,9] While volume holography is effective at multiplexing filters, it does not make for ideal lenses because Bragg selectivity reduces the ability of the element to collect light over a broad angular range, which is crucial for high-numerical aperture imaging.

Instead of using Bragg selectivity, information can be holographically encoded into optical elements using the polarization dependence of subwavelength dielectric structures. This effect is called form birefringence and has previously been realized using linear subwavelength gratings.[10] By locally changing the orientation or the fill factor of the grating, the birefringence of the hologram can be spatially controlled. The ability to control the birefringence of a material has enabled new forms of polarization beam splitters,[10] the generation of nonuniformly polarized light beams,[11] polarization multiplexed Fourier holograms,[12,13] and a high-efficiency multilevel phase lens.[14]

In this Letter, we demonstrate a holographic encoding scheme that utilizes single elliptical nanowires to locally control the form birefringence. Our scheme uses a nanowire pitch of one-quarter of the free space wavelength of the incident light, enabling the

Received: July 8, 2011
Revised: September 14, 2011
Published: September 16, 2011

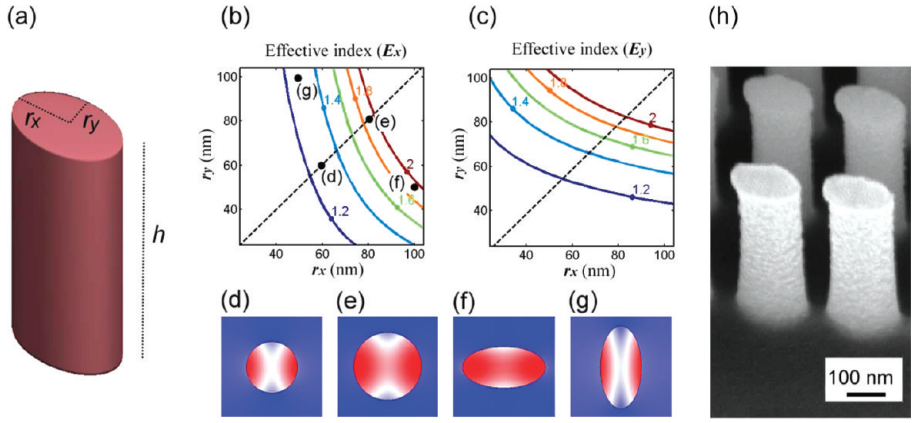

Figure 1. Elliptical nanowire form birefringence. (a) Geometry of an elliptical nanowire. The nanowire has a cross-section defined by the two radii, r_x and r_y, and a height h. (b) Finite element simulations of a periodic array of elliptical nanowires of different cross sections for E_x. The nanowires are composed of amorphous silicon, which has a a bulk refractive index of 3.95 at a wavelength of 980 nm. The contour lines join points with the same mode effective index. (c) Contour lines for E_y. (d−g) Field plots of the distribution of E_x for the four different nanowire geometries: (d) and (g) have the same mode effective index and (e) and (f) have the same mode effective index for E_x. (h) Scanning electron micrograph of fabricated elliptical nanowires of type (f) having r_x = 100 nm and r_y = 50 nm.

control of birefringence with extremely high resolution. Instead of holographically encoding data or images, we use this scheme to encode two lens functions into a single element. Using this design freedom, we implement two reconfigurable imaging systems. The first is the front end of a nonmechanical zoom system, capable of projecting images with two different magnifications. The second is a single aperture stereoscopic lens, capable of projecting images from two different perspectives.

Form birefringent materials in the optical frequency range are challenging to fabricate. Previous efforts have focused on fabricating deep subwavelength gratings, where a large aspect ratio is needed to produce the required polarization-dependent phase shift. Instead of using subwavelength gratings, we demonstrate that elliptical nanowires are also capable of large form birefringence. Many reports have demonstrated that silicon nanowires can be patterned with an extraordinarily large aspect ratio,[15−17] making them an ideal candidate for form birefringence. Using electron beam lithography and reactive ion etching, it is possible to control the cross-sectional shape of each nanowire in the array. Each nanowire can be considered to be a waveguide that has a corresponding effective refractive index (n_{eff}) for each of the two different incident linear polarization states, E_x and E_y. Nanowires that have a circular cross-section have the same n_{eff} for both E_x and E_y polarized incident light. However, nanowires that have an elliptical cross-section have a different n_{eff} for E_x and E_y, which is equivalent to form birefringence.

Our goal is to realize a pattern acting as a two-level phase grating for one polarization and a second completely independent two-level phase grating for the other polarization.[18,12] For each of the two phase functions, light must experience a phase delay that can take one of two values, depending on which of two polarization states it comprises. Four different nanowire structures are therefore needed. The difference between these phase delays should be π, in order to achieve the maximum possible diffraction efficiency for a two level grating of 40.5%. A similar encoding scheme was implemented by Yu et al.[12] to encode holographic images using linear gratings and square arrays of posts and holes. Figure 1 shows the nanowire geometry, which has three geometric degrees of freedom, r_x, r_y, and h. We restrict h to a value of 1 μm because in previous work[17] we developed a reliable fabrication process for silicon nanowires with this height, with radii down to 40 nm. Further details of the nanowire fabrication are included in the Supporting Information.

To find the required dimensions r_x and r_y, we use a finite element method (FEM) mode solver (COMSOL) to evaluate the effect of cross-sectional shape on the form birefringence. The simulated structure is illustrated in Figure 1a. Figure 1b and c shows the results for the effective index of elliptical nanowires with radii r_x and r_y for both polarizations E_x and E_y. The nanowires are composed of amorphous silicon that has a bulk refractive index of 3.95 at a wavelength of 980 nm,[19] and they are placed in a square unit cell with a length 250 nm. Further details of the numerical simulation are included in the Supporting Information. We restrict the parameter search to nanowire radii that support only two modes, corresponding to the lowest order modes that are primarily polarized in X and Y. The contour plots in Figure 1b show that as r_x of the nanowire increases, the n_{eff} for the E_x mode increases dramatically. While, as r_y of the nanowire increases, the effective index of the E_x mode increases much slower. If the effective index of E_x were completely uncoupled from the nanowire radius in Y, then the contour plot would be an array of vertical lines. Instead, the two are coupled slightly, which results in the diagonally curved contours that are shown. The equivalent contour plot of n_{eff} for E_y is also shown (Figure 1c) and is a rotated version of the case of E_x.

We first choose two circular cross-section nanowires, corresponding to points along the dotted diagonal line of Figure 1b. As discussed, the difference in phase delay of a wave traveling through these two structures should ideally be π and will operate equally on both E_x and E_y. This condition is satisfied when Δn_{eff} is equal to $\lambda/2h$ = 0.49. We find that nanowires with radii of 62 and 82 nm satisfy this condition and have n_{eff} values of 1.3 and 1.8, which we call n_{low} and n_{high}, respectively. These are denoted as points (d) and (e) in Figure 1b. The field distributions of the E_x modes for these two nanowires are shown in Figure 1d and e. By periodically arranging these two nanowires, it is possible to realize a polarization-insensitive dielectric grating.[20−22]

Next, we consider the implementation of form birefringence. In this case, an elliptical nanowire with n_{low} for E_x and n_{high} for E_y is needed. The same nanowire will have n_{high} for E_x and n_{low} for E_y,

when rotated by 90°. From inspection of the contours of Figure 1b, we can see that point (f) with r_x and r_y of 100 and 50 nm, respectively, approximately satisfies this criteria and has a n_{eff} of 1.82 and 1.3 for E_x and E_y, respectively. The opposite criteria holds for point (g), with n_{eff} taking values of 1.3 and 1.82 for E_x and E_y, respectively. The field distributions of the E_x modes for the two elliptical nanowires are shown in Figure 1f and g. Using these four nanowire geometries, patterns can be built for which each linear polarization encounters a completely different phase profile. With the nanowire geometries chosen, we next encode them into computer-generated holograms. Two separate desired phase functions for E_x and E_y are first analytically derived, based on the desired application. Each phase function is sampled in two dimensions on a pitch of 250 nm. We then discretize the phase for each incident polarization into one of two values, and the appropriate nanowire geometry for that point is chosen from the four possibilities. The result, a pattern of nanowires on a 250 nm pitch, achieves the goal of a two-level phase grating for one polarization, with a second, independent, two-level phase grating for the other.

To demonstrate and characterize nanowire form birefringence, we first encode test images into arrays of elliptical nanowires. Figure 2a shows a bright field image, obtained with unpolarized light, of a nanowire array where two perpendicular arrows have been polarization multiplexed. The array is designed so that, when the near-field is imaged, only the arrow that is directed along the incident polarization is visible. Figure 2b shows the center of the nanowire array. In regions where the arrows overlap, the nanowires are circular, while in the non-overlapping regions, the nanowires are elliptical and birefringent. The nanowire array is illuminated with polarized infrared light from a near-infrared LED (wavelength λ_0 = 940 nm), with the transmitted light being imaged by an objective lens (50× magnification) onto a CCD camera (Figure 2c and d). Each arrow is only four nanowires wide, slightly larger than the free space wavelength of the illumination, demonstrating the high resolution possible with nanowire form birefringence. The images in Figure 2c and d show good contrast for the arrow pointed along the polarization direction as well as a small amount of contrast for the perpendicular arrow. The presence of the perpendicular arrow is due to polarization cross-talk and is discussed further in the following case.

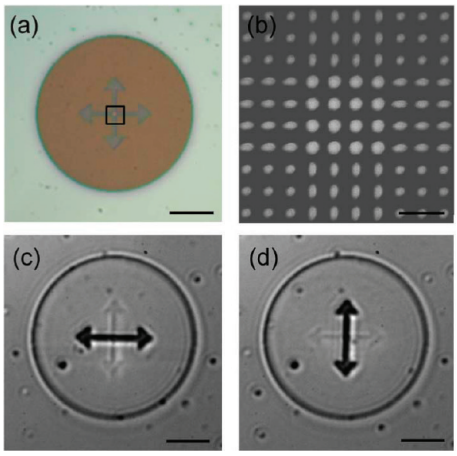

Figure 2. Polarization image multiplexing. (a) Bright field microscope image of nanowire array taken in reflection with unpolarized light (visible wavelengths). (b) Scanning electron micrograph of center of nanowire array, where the two arrows overlap. All four geometries of nanowires can be seen in the image. (c and d) Microscope image (50× objective lens), obtained in trasmission mode, of nanowire array illuminated with an infrared LED (λ_0 = 940 nm). (c) Image when illumination is polarized in E_x and (d) when illumination is polarized in E_y. The scale bars are 10 μm in (a), (c), and (d) and 500 nm in (b).

In addition to images, grating patterns can be encoded to measure the diffraction efficiency of the fabricated nanowire arrays as a function of incident polarization. Figure 3 shows a grating structure designed to diffract E_x vertically and E_y horizontally. The effective period of the grating is 4 μm for both polarizations. By imaging the far field diffraction pattern, we can quantify both the diffraction efficiency and the polarization contrast of the nanowire grating. In this case, the diffraction efficiency is defined as the ratio of the power in the desired diffraction order divided by the power in the total far field, excluding power that is absorbed and reflected. The polarization contrast is defined to be the power in a desired diffraction order relative to the power in an undesired diffraction order. After accounting for the size of the incident beam relative to the nanowire array, we measure diffraction efficiencies of 28.3 and 27.5% for the two horizontal diffraction orders in Figure 3c and 25.1 and 26.5% efficiencies for the two vertical diffraction order shown in Figure 3d. We measure polarization contrasts of 15.3:1 and 26.8:1 for E_y and E_x, respectively. The diffraction efficiencies are somewhat less than the ideal value of 40.5%. The reduction in efficiency is due to different reflection coefficients[23] of the different nanowire geometries and from the difficulty in fabricating the exact nanowires dimensions suggested by FEM simulation. Despite the tight tolerances, the fabricated elliptical nanowire gratings are still more than twice as efficient as amplitude gratings, and additionally, they show high polarization contrast ratios.

Encoding lenses into the nanowire array is similar to encoding images or simple gratings. Phase functions for each multiplexed lens can be defined analytically based on the desired lens properties. Two monochromatic phase functions (φ_1, φ_2) for

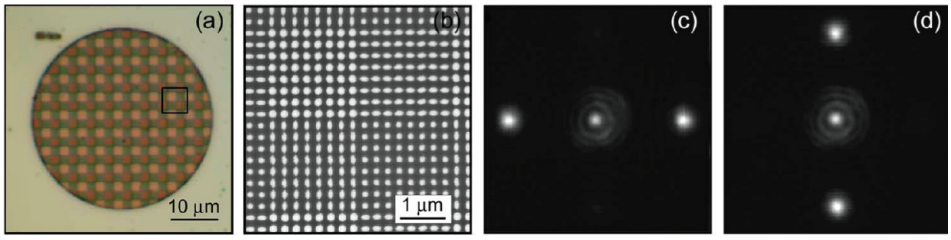

Figure 3. Elliptical nanowire gratings. (a) Bright field microscope image of the two-dimensional elliptical nanowire grating taken in reflection with unpolarized light (visible wavelength). (b) Scanning electron micrograph showing one period of the grating. Repetition of this in both the horizontal and vertical directions yields the grating. (c and d) Images of the far field of the grating when illuminated with a laser beam (λ_0 = 976 nm) that is linearly polarized in (c) E_y and (d) E_x.

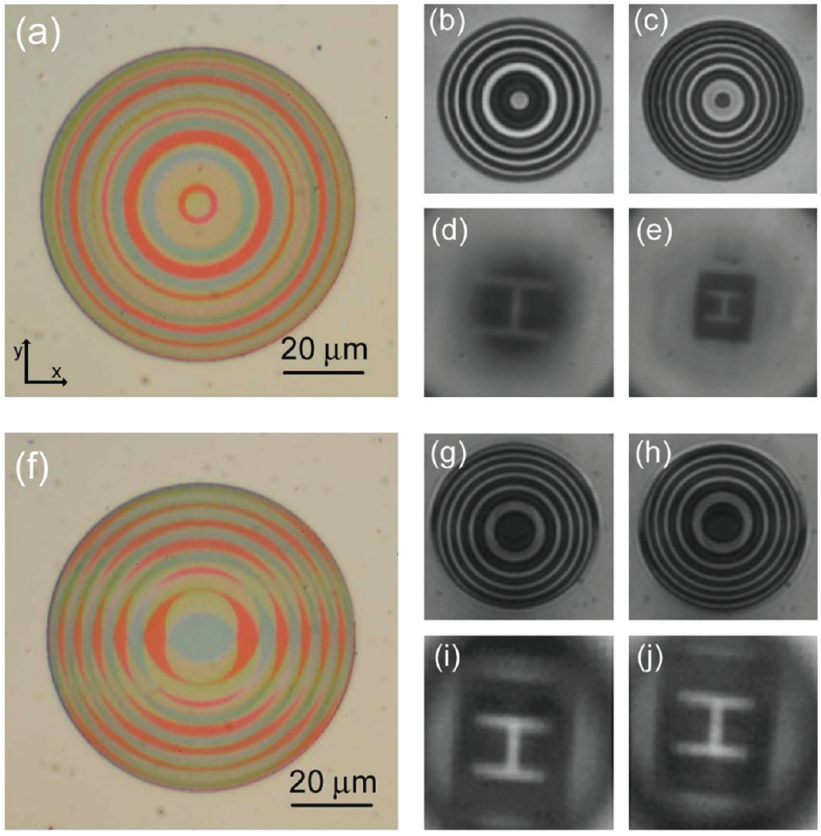

Figure 4. Nanowire multiplexed imaging systems. (a) Microscope image (reflection mode) of nanowire lens with two polarization-encoded focal lengths. (b and c) Images of lens obtained under *x*- and *y*-polarized illumination, respectively. (d and e) Image planes of the lens for *x*- and *y*-polarized illumination, respectively, demonstrating magnifications of 1.12 and 0.59, respectively. (f) Microscope image (reflection mode) of stereoscopic nanowire lens. (g and h) Images of the lens obtained under *x*- and *y*-polarized illumination, respectively. (i and j) Image planes of the lens for *x*- and *y*-polarized illumination, respectively, exhibiting parallax.

nonparaxial lenses defined on a plane can be written as

$$\phi_{1(x,y)} = \exp(-jk\sqrt{(x-x_2)^2 + (y-y_2)^2 + (f_1)^2}) \tag{1a}$$

$$\phi_{2(x,y)} = \exp(-jk\sqrt{(x-x_2)^2 + (y-y_2)^2 + (f_2)^2}) \tag{1b}$$

where k is the wave vector $(2\pi/\lambda)$, x_n and y_n define the position of the optical axis of the lens in the transverse plane, and f_n is the focal length.[24,25] We encode these two phase functions using an array of nanowires, each of which is one of the four elliptical nanowires described previously.

We first investigate a nanowire lens whose focal length depends on the incident polarization. Figure 4a shows a microscope image taken in reflection of this lens. The two encoded lens functions have the same optical axis but have different focal lengths for different polarizations (180 and 120 μm). The focal lengths are chosen so that, at an object to nanowire lens distance of 360 μm, the nanowire lens to image distances for the two polarizations is 360 and 180 μm, respectively. The resulting magnifications are predicted to be 1.0 and 0.5. Figure 4b and c shows images of the lens when illuminated with *x*- and *y*-polarized light, respectively. These images reveal the two diffractive lenses encoded into the nanowire array via polarization. It can be seen that the lens in Figure 4c has more rings and consequently a shorter focal length than the lens in Figure 4b. Figure 4d and e shows the image planes of the nanowire lens. By changing the polarization and then adjusting the position of the relay lens (see Supporting Information Figure 1), we find the optimal focusing conditions which result in magnifications of 1.12 and 0.59. With a single tunable focal length lens, it is not possible to make a nonmechanical zoom system. However, as was recently shown, two tunable focal length lenses can be arranged in a Galilean telescope to realize this goal.[26] The nanowire imaging system demonstrated here can therefore be considered the front end of a nonmechanical zoom system.

The second multiplexed nanowire imaging system is designed for recording stereoscopic image pairs. Stereoscopic imaging enables three-dimensional imaging and traditionally requires two imaging paths collected at a small angular or spatial separation. This is most frequently done using two spatially offset lenses but can also be performed by spatially dividing the aperture of a single lens. Our multiplexed imaging method enables the capture of two stereoscopic images from the same aperture of a single lens without any subdivision. Figure 4f shows the stereoscopic lens, where the focal length is 150 μm for both polarizations, but the optical axis of each lens is offset from the center by 3 μm vertically. Figure 4g−j shows images of the stereoscopic lens and its image plane for both illumination polarizations. The images

show parallax, which is a function of the optical axis offset between the two multiplexed nanowire lenses and the nanowire lens to object distance. Using the measured parallax and the known lens properties, we calculate the distance from the lens to the object to be 430 μm (see Supporting Information). This compares reasonably well to the distance of 400 μm determined from the image size and the known object size. The parallax method for distance determination, however, does not require the object size to be known. Unlike other microscopes demonstrated recently that use parallax,[27,28] this method requires no registration between the image pairs, and the only shift observed on the image sensor is from the parallax. In addition, the quality of the image is not degraded by subdividing the back aperture.

In this paper, we have demonstrated a method to encode phase patterns into arrays of elliptical nanowires. Using the differential effective mode index of elliptical nanowires, we have shown that two phase patterns can be polarization encoded into a single array of elliptical cross-section nanowires. While we have demonstrated only two level phase gratings, it is possible to obtain higher diffraction efficiency with additional phase levels. A three level phase grating having a possible diffraction efficiency of 68% could be made in the same way. It would require, however, nine different nanowire geometries instead of four.

This method of polarization multiplexing is particularly useful in microoptical imaging systems, where it is traditionally difficult to dynamically adjust imaging properties. We have demonstrated two imaging systems that benefit from polarization multiplexing, the front half of a nonmechanical zoom and a stereoscopic lens. Further advances in nanofabrication techniques and phase encoding methods will continue to expand the capabilities of microoptical imaging systems.

■ ASSOCIATED CONTENT

Supporting Information. Additional information and figures. This material is available free of charge via the Internet at http://pubs.acs.org.

■ AUTHOR INFORMATION

Corresponding Author

*E-mail: schonbrun@rowland.harvard.edu. Telephone: 617-497-4704.

■ ACKNOWLEDGMENT

The study was supported by the Rowland Junior Fellows program. Fabrication work was performed at the Harvard Center for Nanoscale Systems (CNS), which is supported by the National Science Foundation. K.S. acknowledges support from Zena Technologies.

■ REFERENCES

(1) Lohmann, A. W. *Appl. Opt.* **1989**, *28*, 4996–4998.
(2) Rosen, J.; Brooker, G. *Nat. Photonics* **2008**, *2*, 190–195.
(3) Hanley, Q. S.; Verveer, P. J.; Gemkow, M. J.; Arndt-Jovin, D.; Jovin, T. M. *J. Microsc.* **1999**, *196*, 317–331.
(4) Booth, M. J.; Neil, M. A. A.; Juskaitis, R.; Wilson, T. *Proc. Nat. Acad. Sci. U.S.A.* **2002**, *99*, 5788–5792.
(5) Kuiper, S.; Hendriks, B. H. W. *Appl. Phys. Lett.* **2004**, *85*, 1128–1130.
(6) Heanue, J. F.; Bashaw, M. C.; Hesselink, L. *Science* **1994**, *265*, 749–752.
(7) Blanche, P. A.; Bablumian, A.; Voorakaranam, R.; Christenson, C.; Lin, W.; Gu, T.; Flores, D.; Wang, P.; Hsieh, W. H.; Kathaperumal, M.; Rachwal, B.; Siddiqui, O.; Thomas, J.; Norwood, R. A.; Yamamoto, M.; Peyghambarian, N. *Nature* **2010**, *468*, 80–83.
(8) Liu, W.; Psaltis, D.; Barbastathis, G. *Opt. Lett.* **2002**, *27*, 854–856.
(9) Luo, Y.; Oh, S. B.; Barbastathis, G. *Opt. Lett.* **2010**, *35*, 781–783.
(10) Xu, F.; Tyan, R. C.; Sun, P. C.; Fainman, Y.; Cheng, C. C.; Scherer, A. *Opt. Lett.* **1996**, *21*, 1513–1515.
(11) Davidson, N.; Friesem, A. A.; Hasman, E. *Opt. Lett.* **1992**, *17*, 1541–1543.
(12) Yu, W.; Konishi, T.; Hamamoto, T.; Toyota, H.; Yotsuya, T.; Ichioka, Y. *Appl. Opt.* **2002**, *41*, 96–100.
(13) Cai, W.; Libertun, A. R.; Piestun, R. *Opt. Express* **2006**, *14*, 3785–3791.
(14) Hasman, E.; Kleiner, V.; Biener, G.; Niv, A. *Appl. Phys. Lett.* **2003**, *82*, 328–330.
(15) Huang, Z.; Zhang, X.; Reiche, M.; Liu, L.; Lee, W.; Shimizu, T.; Senz, S.; Gosele, U. *Nano Lett.* **2008**, *8*, 3046–3051.
(16) Garnett, E.; Yang, P. *Nano Lett.* **2010**, *10*, 1082–1087.
(17) Seo, K.; Wober, M.; Steinvurzel, P.; Schonbrun, E.; Dan, Y.; Ellenbogen, T.; Crozier, K. B. *Nano Lett.* **2011**, *11*, 1851–1856.
(18) Ford, J. E.; Xu, F.; Urquhart, K.; Fainman, Y. *Opt. Lett.* **1993**, *18*, 456–458.
(19) de Dood, M. J. A.; Polman, A.; Zijlstra, T.; van der Drift, E. W. J. M. *J. Appl. Phys.* **2002**, *92*, 649–653.
(20) Stork, W.; Striebl, N.; Haidner, H.; Kipfer, P. *Opt. Lett.* **1991**, *16*, 1921–1923.
(21) Chen, F. T.; Craighead, H. G. *Opt. Lett.* **1996**, *21*, 177–179.
(22) Freese, W.; Kampfe, T.; Kley, E. B.; Tunnermann, A. *Opt. Lett.* **2010**, *35*, 676–678.
(23) Richter, I.; Sun, P. C.; Xu, F.; Fainman, Y. *Appl. Opt.* **1995**, *34*, 2421–2429.
(24) Schonbrun, E.; Rinzler, C.; Crozier, K. B. *Appl. Phys. Lett.* **2008**, *92*, 071112.
(25) Schonbrun, E.; Abate, A. R.; Steinvurzel, P. E.; Weitz, D. A.; Crozier, K. B. *Lab Chip* **2010**, *10*, 852–856.
(26) Valley, P.; Dodge, M. R.; Schwiegerling, J.; Peyman, G.; Peyghambarian, N. *Opt. Lett.* **2010**, *35*, 2582–2584.
(27) Sun, Y.; McKenna, J. D.; Murray, J. M.; Ostap, E. M.; Goldman, Y. E. *Nano Lett.* **2009**, *9*, 2676–2682.
(28) Bowman, R.; Gibson, G.; Padgett, M. *Opt. Express* **2010**, *18*, 11785–11790.